Block copolymers

Well-Ordered Thin-Film Nanopore Arrays Formed Using a Block-Copolymer Template**

*Yeon Sik Jung and Caroline A. Ross**

Following Moore's law, the transistor density and hence the computing power of integrated circuits have scaled exponentially with time.[1] However, optical lithography technology, which has sustained Moore's law over the last half century, is reaching a limit in pattern resolution. Unconventional lithography techniques are therefore required to enable the next generations of microelectronic device fabrication. The critical requirements are scalability, high throughput, low cost, and compatibility with existing fabrication techniques.

During the past decade, films of self-assembled diblock copolymers (BCPs) have attracted significant attention for lithography applications because they can generate ordered microdomains with sizes below 30 nm by thermodynamically driven microphase separation[2–16] In this application, 2D arrays or monolayers of microdomains are desirable to facilitate pattern transfer.[4,7,13,14,17] Typically, self-assembled BCP microdomain arrays possess only short-range order, and thus to make technologically useful structures with long-range order and accurate registration, BCPs may be templated using features formed by another lithography technique.[4,5,9,10,13–15,17,18] The most common templates are chemical[5,15,19,20] or topographic[4,8,9,13,14,17] patterns defined by electron beam lithography or optical lithography. Chemical templates can regulate the orientation and position of BCP microdomains to high precision[5,15,19,20] in BCP films consisting of out-of-plane cylinders or lamellae, in which both blocks contact the chemically patterned substrate. Topographic patterns, with or without substrate surface functionalization, use spatial confinement to impose long-range ordering in BCPs of many morphologies including in-plane cylinders and spheres,[4,8,9,13,14,17] and can also form 3D assemblies,[21–24] including morphologies such as rings, spirals, disks, and hollow cylinders that are not found in bulk.[21–23,25,26]

Of key importance is the ability to transfer patterns with good fidelity from block copolymers into a variety of materials, including metals that may be difficult to dry-etch. In this communication, we describe a simple route to fabricate thin films with well-ordered nanopores (antidot arrays) using self-assembled block-copolymer lithography and pattern transfer processes. Long-range ordering of a sphere-forming block copolymer is accomplished using a brush-coated 1D topographic template and solvent annealing, and the spheres are used to make nanoporous patterns through a pattern reversal process. Examples of Ti, Pt, Ta, W, silica, and magnetic Co and Ni antidot arrays are presented. A second image reversal process was used to form Ni dot arrays. This general method may be used to make a diverse range of nanoatterned films that can be useful in applications including via formation in integrated circuits, filters, plasmonic and photonic bandgap structures, catalysts, templates, sensors, and solar cells.[27–35]

The fabrication process for nanoporous metallic thin films is illustrated in Figure 1. A sphere-forming polystyrene-*b*-poly(dimethylsiloxane) (PS-PDMS) BCP was used to make nanoscale dot arrays. PS-PDMS (Figure 1a) has excellent microdomain ordering due to its large Flory–Huggins interaction parameter compared to other commonly used BCPs. It also has good etch selectivity between the two blocks due to the inorganic component (Si) in the PDMS.[13,14,26] An UV interference lithography system was employed to make 1.2-μm-period linear trenches with a depth of 40 nm (Figure 1b) that were then treated with a PDMS brush. A disordered 30-nm-thick PS-PDMS thin film was obtained by spin-coating a 1.5% toluene solution of the BCP onto the patterned substrate (Figure 1c), then the film was annealed in a toluene solvent vapor to obtain an equilibrium microdomain morphology (Figure 1d) consisting of a monolayer of close-packed PDMS spheres in a PS matrix sandwiched between thin PDMS brush layers at the film–substrate and film–air interfaces.[13,14,26] For simplicity, the thin PDMS layers are not shown in Figure 1d. Etching by CF_4 plasma followed by O_2 plasma removes the PS matrix and oxidizes the PDMS spheres (Figure 1e). A 55–70-nm-thick metal film was sputter-deposited on top of the PDMS (Figure 1f) and etched using CF_4 plasma. This slowly removes the metal, primarily by sputter-etching, until the oxidized PDMS is exposed, which is then etched quickly by forming volatile SiF_x.[26] Thus, the final morphology is a reverse image of the original PDMS dot patterns (Figure 1g). The detailed patterning mechanism will be discussed below.

Figure 2a–c shows scanning electron microscopy (SEM) images of self-assembled PDMS spheres in the trenches after removing the PS. The average diameter of the structures is 17.9 ± 1.1 nm, and the average center-to-center distance is 35.0 ± 1.5 nm. Each 960-nm-wide trench templates 32 rows of hexagonally ordered dots, and Figure 2d shows the fast Fourier transform of the image. The height of the dots is around 10–

[*] Prof. C. A. Ross, Y. S. Jung
Department of Materials Science and Engineering
Massachusetts Institute of Technology
Cambridge, MA 02139 (USA)
E-mail: caross@mit.edu

[**] The support of the Semiconductor Research Corporation is gratefully acknowledged.

DOI: 10.1002/smll.200900053

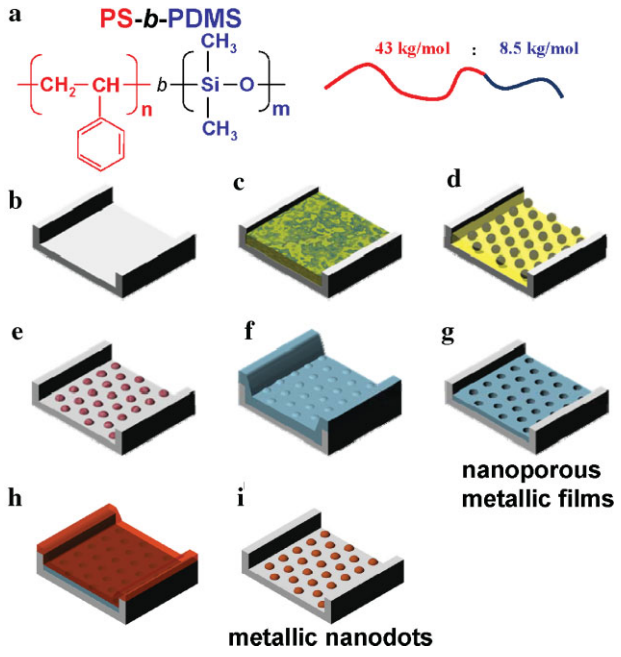

Figure 1. Schematic representation of the fabrication process. a) The chemical structure of the PS-PDMS block copolymer, b) a lithographically-patterned trench, c) a spin-coated block-copolymer film in the trench, d) well-ordered block-copolymer microdomain array after solvent-annealing, e) an array of oxidized PDMS dots after CF_4 and O_2 reactive ion etching processes, f) a metal film deposited on the dot array, and g) a porous metallic film after a high-power CF_4 plasma etching. The porous film can be used for Ni dot fabrication by employing a second pattern-reversal step. h) Ni film deposition and i) a high-power CF_4 plasma etching reveals the Ni dot array.

11 nm. For each trench the close-packed directions of the array align parallel to the trench walls, which is consistent with previous reports.[8,18] The close-packed orientation, which has the lowest free energy at the brush-coated wall/BCP interface due to the minimization of chain stretching by maximizing the number of spheres near the brush,[18] first aligns parallel with the trench walls and propagates during self-assembly. However, for narrow trenches with incommensurate widths, different orientations, where the closed-packed direction is rotated from the trench wall, are also observed, probably due to the dominant effect of strain energy in incommensurate templates.

Ordering was achieved within 20 min solvent annealing time, which is faster than the previously reported solvent annealing times required for sphere-forming BCPs.[36–38] The very low surface energy of the PDMS brush adsorbed on the substrate may enhance the chain mobility, contributing to the fast self-assembly. In general, the throughput of block copolymer nanolithography is believed to be limited by the annealing process, but this result suggests that annealing time may be reduced by employing solvent annealing and a brush treatment.

The well-ordered dot patterns were converted into a nanoporous metallic thin film via a pattern reversal process. Figure 3a and b shows images of a 55-nm-thick Pt thin film deposited on the oxidized PDMS patterns with a topography indicative of the buried BCP patterns. A 450 W CF_4 plasma treatment was used to thin the deposited metallic film through a physical sputtering process since fluorides of most of the metals used here, Pt, Ti, Ta, Co, and Ni, have a boiling point higher than room temperature, and thus they are nonvolatile.[39] The only exception is W, which forms volatile WF_6 with a boiling point of 17.1 °C.[39] After 5 min of CF_4 plasma etching, the Pt surface becomes smooth as shown in Figure 3c. The etch rates for W, Ti, Ta, Pt, Ni, and Co were approximately 25, 11.4, 10, 3.5, 2.5, and 2.3 nm min^{-1}, respectively. When the thickness of the remaining thin film is around 10 nm, the oxidized PDMS patterns are exposed to the reactive plasma and are rapidly etched away by forming volatile SiF_x species. As a result, a nanoporous metallic film ≈8–10-nm-thick with the reverse image of the original block copolymer pattern was obtained. Figure 3d shows Pt, W, Ti, and Ta films with hexagonally arranged nanopores. The histograms in Figure 4a show the comparison between the dimensions of the original BCP pattern and the pores formed in the Ti film. The average pore size is 16.8 ± 1.4 nm, which is 6% smaller than that of the BCP template. The formation of metal oxides, which are not chemically etchable with F ions, at the boundary between the deposited metal and oxidized PDMS microdomain may contribute to pore shrinkage. This pattern transfer method can be applied to other morphology block copolymers, for example the forma-

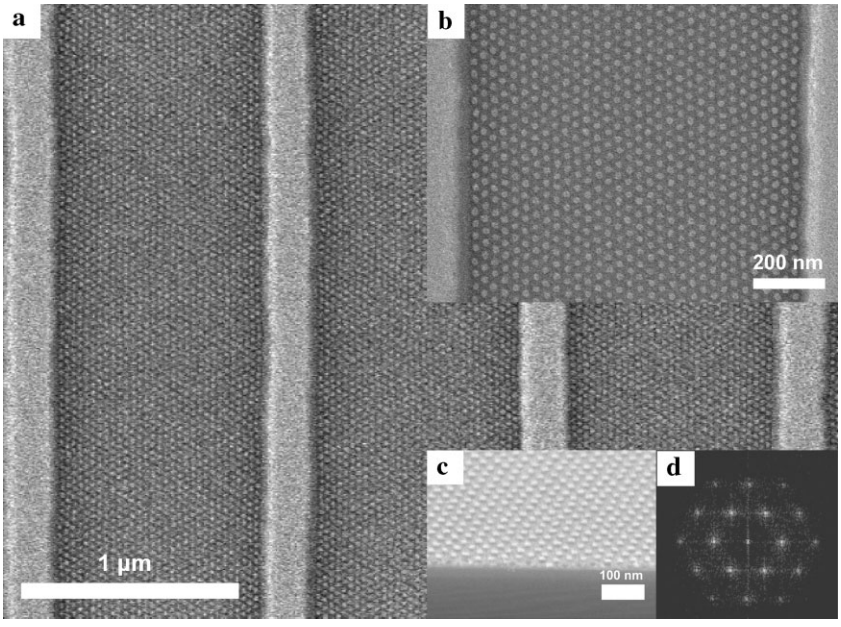

Figure 2. a–c) SEM images of self-assembled block-copolymer patterns after reactive ion etching. The oxygen plasma selectively removes the PS matrix block and oxidizes the PDMS spheres. d) The fast Fourier transform (FFT) of (b).

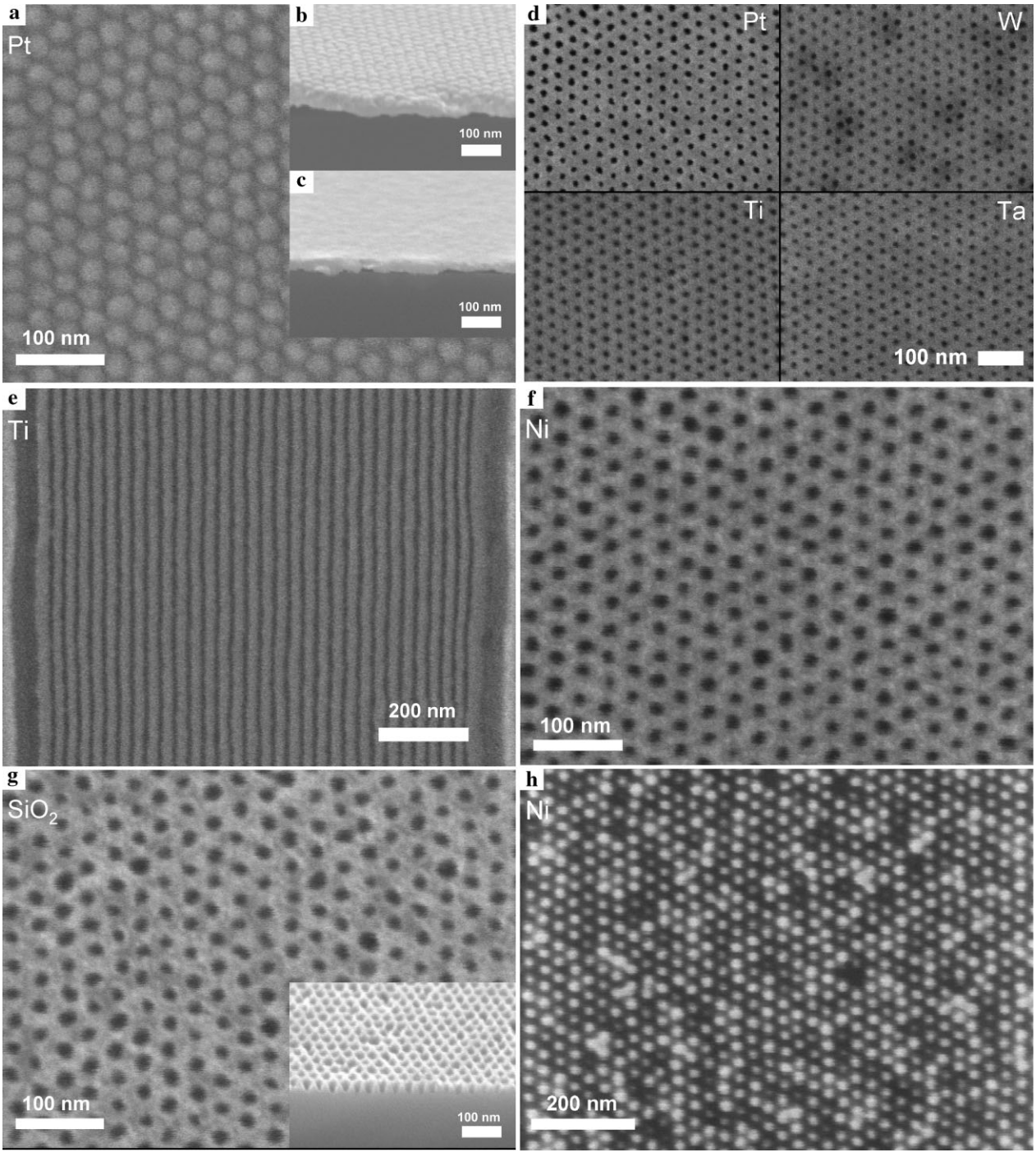

Figure 3. SEM images of a and b), a Pt thin film sputter-deposited on oxidized PDMS spheres, c) smoothed surface of the Pt after a high-power CF_4 plasma treatment, d) various metallic thin films with nanopores after the selective removal of the PDMS template, e) Ti nanowire patterns, f) a nanoporous Ni film on SiO_2, g) patterned SiO_2 via CF_4 reactive ion etching and Ni wet-etching, and h) a Ni dot array.

tion of concentric metal rings,[26] or metal nanowires formed from a cylinder-morphology BCP (Figure 3e), which are described elsewhere.[40]

We now discuss the ferromagnetism of porous Co films with ≈15-nm-diameter pores. Figure 4b shows the magnetic hysteresis loops of the antidot array compared to that of an unpatterned film of the same thickness made by CF_4-etching a film on a smooth substrate. The inset presents the morphology of Co antidots. The significant increase in coercivity of the antidot film (220 Oe) compared to that of the unpatterned film (8 Oe) is a result of pinning of domain walls by the pores,[41–44] as observed in other magnetic antidot arrays made by ion-milling[42] or by deposition onto porous structures such as anodized alumina or block copolymer films.[43,44] Co nanowire arrays resembling Figure 3e also have a coercivity (255 Oe) much greater than that (8 Oe) of the unpatterned film (not

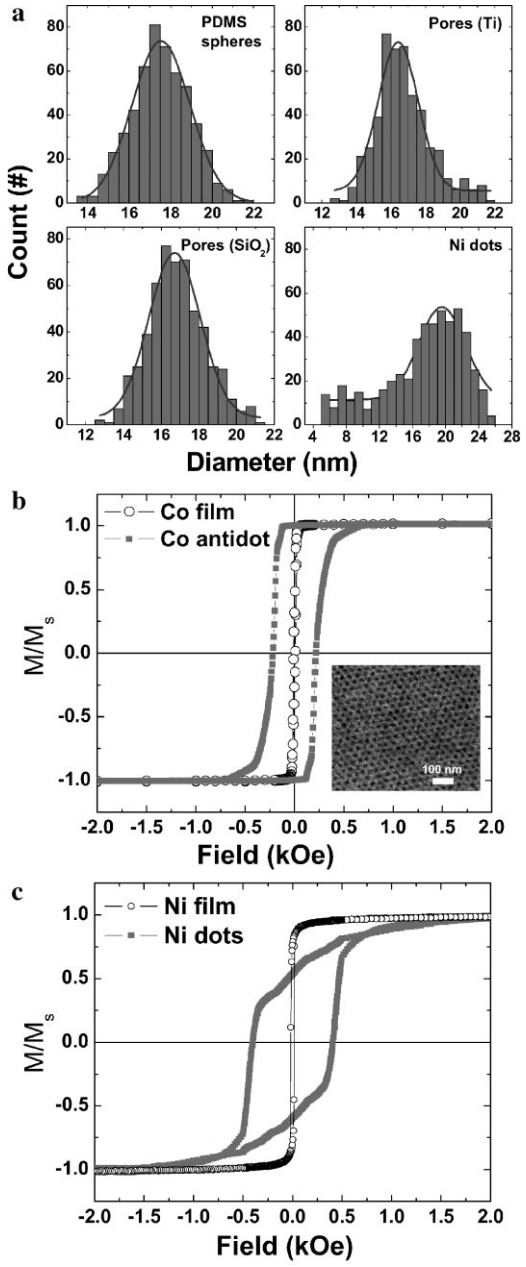

Figure 4. a) Size histograms of PDMS dots, pores formed in Ti and SiO_2, and Ni dots. The magnetic hysteresis loops of b) a Co antidot pattern and c) Ni dots, compared with the hysteresis of unpatterned Ni and Co thin films.

shown here) and exhibit a strong in-plane magnetic shape anisotropy. These observations are consistent with uniform pattern transfer over the sample area of several square centimeters.

The etch rate of SiO_2 is comparable with that of the oxidized PDMS, and thus the pattern-reversal technique cannot be used to make a porous silica film. Instead, nanoporous metallic films can be used as a robust etch mask to make holes in an underlying 20-nm-thick SiO_2 film. A patterned Ni film with pore diameter 15.7 ± 1.8 nm (Figure 3f) was used as a mask to etch the SiO_2 film using a CF_4 plasma at a power of 180 W, then the remaining Ni mask pattern was removed with a nickel wet etchant. Figure 3g shows the top and cross-sectional views of the porous SiO_2 pattern, in which the average hole size was 14.2 ± 2.1 nm (see the histogram in Figure 4a). Materials such as porous silica can be useful as a low-k interlayer dielectric. This simple technique may be extended to the generation of well-controlled pores in other oxide materials such as TiO_2, which can be used for dye-sensitized solar cell devices.

Finally, metallic Ni dot patterns were formed by a double pattern-reversal process (Figure 1g–i). This process avoids the need for ion-beam etching to form magnetic dot arrays, as demonstrated previously.[45] Nanoporous Ti films were first prepared as described in Figure 1b–g. Ti was chosen since it has a higher etch rate than Ni. A 70-nm-thick Ni film was then sputter-deposited onto the Ti, filling the pores, and a subsequent 450 W CF_4 plasma treatment was used to form the Ni dot array. As the Ni is eroded, the Ti antidot array is revealed, which is then rapidly removed due to its 4.5 times greater etch rate compared to Ni. Figure 3h demonstrates the Ni dots that have an average diameter of 17.3 ± 4.9 nm. The increase in size distribution compared to both the original BCP patterns and the pores in the Ti template may result from the inhomogeneity of the polycrystalline film microstructure, or from edge roughness that develops during pattern transfer, and might be improved via the microstructure of the Ni and Ti layers. Another approach would be to use a perforated lamellar geometry PS-PDMS film,[46] which would form dot arrays after a single pattern-reversal step. The magnetic hysteresis loop shown in Figure 4c shows a coercivity of 417 Oe for the dot array, compared to 17 Oe for the continuous thin film, consistent with single domain reversal. This method may be suitable for generating nanoparticle arrays for patterned media if the size distribution is improved.[47,48]

In summary, we have demonstrated generation of ordered arrays of nanoscale holes in various metallic thin films by using a mask made from a 35-nm-period, 18-nm-sphere-diameter spherical morphology block copolymer film and a CF_4 plasma etching process that sputter-etches the metal films. This method is versatile and has been used to form antidot arrays in a variety of metals including Ti, Pt, W, Ta, Co, and Ni, as well as Ni dot arrays and Co and Ni line arrays. Ti antidot arrays show a standard deviation in pore diameters of 1.4 nm, compared to 1.1 nm for the block copolymer spheres, illustrating good fidelity in pattern transfer. Ni dots and Co antidots showed a considerably enhanced coercivity compared to unpatterned films, consistent with their confined geometries. Nanoporous metallic thin films were also used as an etch mask to pattern an underlying oxide layer. This simple method can make metallic and oxide thin films with well-ordered holes or dot arrays from a wide range of materials that can be employed in catalysts, dielectrics, magnetic recording, and many other applications.

Experimental Section

Self-assembly of block copolymers: Si substrates with 40-nm-deep trenches with a periodicity of 1.2 μm were fabricated using a Lloyd's Mirror interference lithography system with a He-Cd laser

($\lambda = 325$ nm).[13] The direct and reflected laser beams exposed grating patterns into a 200-nm-thick PFI-88 photoresist (Sumitomo Chemical Co.), which were transferred into the Si substrates through a CF_4 reactive ion etching with a working pressure of 10 mTorr and a power of 200 W. The native oxide surfaces were treated by hydroxy-terminated PDMS homopolymer with molecular weight 5 kg mol^{-1}, which was spun-cast on the substrates and annealed at 170 °C for 15 h, then washed with toluene to remove unreacted polymers, leaving a 3–4-nm-thick grafted PDMS layer.[13] A sphere-forming PS-PDMS BCP (Polymer Source, Inc.) with total molecular weight of 51.5 kg mol^{-1}, minority block volume fraction $f_{PDMS} = 16.5\%$, and polydispersity index of 1.04 was used. BCP thin films with a thickness of 30 nm were obtained by spin-casting toluene solutions of 1.5% by weight of the block copolymer on the substrates, then the BCP films were treated with toluene vapor at room temperature for 20 min. The annealed film was treated with a 5 s, 50 W CF_4 plasma followed by a 22 s, 90 W O_2 plasma to remove the PDMS surface layer and selectively eliminate the PS block, which reveals oxidized PDMS microdomains in the trenches.[13]

Fabrication of nanoporous films and magnetic characterization: Metallic thin films such as Pt, Ti, W, Ta, Co, and Ni with a thickness of 55–70 nm were deposited using a radiofrequency sputtering system (base pressure $= 1 \times 10^{-8}$ Torr, working pressure $= 2 \times 10^{-3}$ Torr, and power = 300 W) on top of the block copolymer patterns and etched with a 450 W 10 mTorr CF_4 plasma for 2–25 min depending on the etch rate and film thickness. Initially the metallic films were slowly sputter-etched by ionized CF_x species, but after the buried block copolymer patterns were exposed to the plasma, they were removed much faster than the metallic films by forming by forming volatile SiF_x.[26] As a result, various nanoporous metallic films were obtained. A nanoporous Ni pattern was transferred into a 20-nm-thick silica film using a 200 W CF_4 plasma. After the completion of etching, the Ni mask was removed with a sulfuric-acid-based nickel etchant at a temperature of 50 °C. A patterned Ti template was used for making Ni dots by depositing a 70-nm-thick Ni film onto the Ti and performing the pattern-reversal process once more. Magnetic hysteresis loops of a porous Co film and Ni dot patterns were obtained using a vibrating sample magnetometer (ADE, model 1660) at room temperature. The surface morphologies of samples were observed using a Zeiss/Leo Gemini 982 SEM operated with an acceleration voltage of 5 kV. A thin layer of AuPd alloy was sputter-coated on the samples in order to avoid charging effects.

Keywords:
block copolymers · magnetic dots · nanolithography · nanoporous films · self-assembly

[1] G. E. Moore, *Electronics* **1965**, *38*, 114.
[2] M. Park, C. Harrison, P. M. Chaikin, R. A. Register, D. H. Adamson, *Science* **1997**, *276*, 1401.
[3] T. Thurn-Albrecht, J. Schotter, C. A. Kastle, N. Emley, T. Shibauchi, L. Krusin-Elbaum, K. Guarini, C. T. Black, M. T. Tuominen, T. P. Russell, *Science* **2000**, *290*, 2126.
[4] J. Y. Cheng, C. A. Ross, E. L. Thomas, H. I. Smith, G. J. Vancso, *Adv. Mater.* **2003**, *15*, 1599.
[5] S. O. Kim, H. H. Solak, M. P. Stoykovich, N. J. Ferrier, J. J. de Pablo, P. F. Nealey, *Nature* **2003**, *424*, 411.
[6] R. A. Segalman, A. Hexemer, E. J. Kramer, *Phys. Rev. Lett.* **2003**, *91*, 196101.
[7] C. T. Black, O. Bezencenet, *IEEE Trans. Nanotechnol.* **2004**, *3*, 412.
[8] J. Y. Cheng, A. M. Mayes, C. A. Ross, *Nat. Mater.* **2004**, *3*, 823.
[9] D. Sundrani, S. B. Darling, S. J. Sibener, *Nano Lett.* **2004**, *4*, 273.
[10] C. T. Black, *Appl. Phys. Lett.* **2005**, *87*, 163116.
[11] C. T. Black, R. Ruiz, G. Breyta, J. Y. Cheng, M. E. Colburn, K. W. Guarini, H. C. Kim, Y. Zhang, *IBM J. Res. Dev.* **2007**, *51*, 605.
[12] S. B. Darling, *Prog. Polym. Sci.* **2007**, *32*, 1152.
[13] Y. S. Jung, C. A. Ross, *Nano Lett.* **2007**, *7*, 2046.
[14] I. Bita, J. K. W. Yang, Y. S. Jung, C. A. Ross, E. L. Thomas, K. K. Berggren, *Science* **2008**, *321*, 939.
[15] R. Ruiz, H. M. Kang, F. A. Detcheverry, E. Dobisz, D. S. Kercher, T. R. Albrecht, J. J. de Pablo, P. F. Nealey, *Science* **2008**, *321*, 936.
[16] F. S. Bates, G. H. Fredrickson, *Annu. Rev. Phys. Chem.* **1990**, *41*, 525.
[17] R. A. Segalman, H. Yokoyama, E. J. Kramer, *Adv. Mater.* **2001**, *13*, 1152.
[18] R. A. Segalman, A. Hexemer, E. J. Kramer, *Macromolecules* **2003**, *36*, 6831.
[19] L. Rockford, S. G. J. Mochrie, T. P. Russell, *Macromolecules* **2001**, *34*, 1487.
[20] M. P. Stoykovich, M. Muller, S. O. Kim, H. H. Solak, E. W. Edwards, J. J. de Pablo, P. F. Nealey, *Science* **2005**, *308*, 1442.
[21] K. Shin, H. Q. Xiang, S. I. Moon, T. Kim, T. J. McCarthy, T. P. Russell, *Science* **2004**, *306*, 76.
[22] Y. Y. Wu, G. S. Cheng, K. Katsov, S. W. Sides, J. F. Wang, J. Tang, G. H. Fredrickson, M. Moskovits, G. D. Stucky, *Nat. Mater.* **2004**, *3*, 816.
[23] H. Q. Xiang, K. Shin, T. Kim, S. I. Moon, T. J. McCarthy, T. P. Russell, *Macromolecules* **2004**, *37*, 5660.
[24] V. P. Chuang, J. Y. Cheng, T. A. Savas, C. A. Ross, *Nano Lett.* **2006**, *6*, 2332.
[25] B. Yu, P. C. Sun, T. C. Chen, Q. H. Jin, D. T. Ding, B. H. Li, A. C. Shi, *Phys. Rev. Lett.* **2006**, *96*, 138306.
[26] Y. S. Jung, W. Jung, C. A. Ross, *Nano Lett.* **2008**, *8*, 2975.
[27] N. K. Raman, M. T. Anderson, C. J. Brinker, *Chem. Mater.* **1996**, *8*, 1682.
[28] V. S. Y. Lin, K. Motesharei, K. P. S. Dancil, M. J. Sailor, M. R. Ghadiri, *Science* **1997**, *278*, 840.
[29] K. P. S. Dancil, D. P. Greiner, M. J. Sailor, *J. Am. Chem. Soc.* **1999**, *121*, 7925.
[30] J. Y. Ying, C. P. Mehnert, M. S. Wong, *Angew. Chem, Int. Ed.* **1999**, *38*, 56.
[31] K. Hara, T. Horiguchi, T. Kinoshita, K. Sayama, H. Sugihara, H. Arakawa, *Sol. Energy Mater. Sol. Cells* **2000**, *64*, 115.
[32] J. S. Seo, D. Whang, H. Lee, S. I. Jun, J. Oh, Y. J. Jeon, K. Kim, *Nature* **2000**, *404*, 982.
[33] P. Jiang, J. F. Bertone, V. L. Colvin, *Science* **2001**, *291*, 453.
[34] Z. S. Wang, C. H. Huang, Y. Y. Huang, Y. J. Hou, P. H. Xie, B. W. Zhang, H. M. Cheng, *Chem. Mater.* **2001**, *13*, 678.
[35] S. Niwa, M. Eswaramoorthy, J. Nair, A. Raj, N. Itoh, H. Shoji, T. Namba, F. Mizukami, *Science* **2002**, *295*, 105.
[36] S. Park, B. Kim, O. Yavuzcetin, M. T. Tuominen, T. P. Russell, *ACS Nano* **2008**, *2*, 1363.
[37] C. B. Tang, J. Bang, G. E. Stein, G. H. Fredrickson, C. J. Hawker, E. J. Kramer, M. Sprung, J. Wang, *Macromolecules* **2008**, *41*, 4328.
[38] Y. Wang, X. D. Hong, B. Q. Liu, C. Y. Ma, C. F. Zhang, *Macromolecules* **2008**, *41*, 5799.
[39] *CRC Handbook of Chemistry and Physics*, 88th ed. *(Internet Version 2008)* (Ed.: D. R. Lide,), CRC Press/Taylor and Francis, Boca Raton, FL **2008**.
[40] Y. S. Jung, E. Verploegen, C. Nam, P. T. Hammond, C. A. Ross, unpublished results.
[41] J. A. Barnard, A. Butera, H. Fujiwara, V. R. Inturi, J. D. Jarratt, T. J. Klemmer, T. W. Scharr, J. L. Weston, *J. Appl. Phys.* **1997**, *81*, 5467.

[42] T. Kubo, J. S. Parker, M. A. Hillmyer, C. Leighton, *Appl. Phys. Lett.* **2007**, *90*, 233113.
[43] V. P. Chuang, W. Jung, C. A. Ross, J. Y. Cheng, P. Oun-Ho, K. Ho-Cheol, *J. Appl. Phys.* **2008**, *103*, 074307.
[44] N. P. Nguyen, S. L. Lim, F. Xu, Y. G. Ma, C. K. Ong, *J. Appl. Phys.* **2008**, *104*, 093708.
[45] J. Y. Cheng, C. A. Ross, V. Z. H. Chan, E. L. Thomas, R. G. H. Lammertink, G. J. Vancso, *Adv. Mater.* **2001**, *13*, 1174.
[46] Y. S. Jung, C. A. Ross, *Adv. Mater.* **2009**, DOI: 10.1002/adma.200802855.
[47] C. Ross, *Annu. Rev. Mater. Res.* **2001**, *31*, 203.
[48] C. A. Ross, J. Y. Cheng, *MRS Bull.* **2008**, *33*, 838.

Received: January 9, 2009
Revised: February 23, 2009
Published online: March 30, 2009

